

## AFM of Poly(vinyl alcohol) Crystals Next to an Inorganic Surface

K. E. Strawhecker and E. Manias\*

*Department of Materials Science and Engineering, The Pennsylvania State University, 325-D Steidle Bldg, University Park, Pennsylvania 16802**Received January 31, 2001*

**ABSTRACT:** Crystallization of poly(vinyl alcohol) in the presence of an inorganic filler surface (sodium montmorillonite, MMT) was observed and compared to the crystallization of the neat polymer. For this purpose, several atomic force microscopy modes, providing spatial resolution between amorphous and crystalline polymer, are employed to observe filled and unfilled PVA films. The various AFM modes utilized are detailed, with the emphasis on how they can contrast stiff (crystalline) and softer (amorphous) domains on a polymer surface. The study revealed changes in the PVA crystal morphology, with bulk crystallites growing to sizes of more than 5  $\mu\text{m}$ , whereas next to the inorganic surfaces grow to only 1–2  $\mu\text{m}$  in size. Moreover, complementary X-ray diffraction and DSC investigations indicate a new crystal structure formed next to the MMT surfaces, at the expense of the bulklike crystal.

**Introduction**

The crystallization of polymers next to inorganic surfaces has been studied extensively.<sup>1</sup> Many of these studies have shown a nucleating or epitaxial effect of the inorganic surface,<sup>2–5</sup> oftentimes stabilizing a crystalline phase which is rarely found in the bulk polymer. This effect can be used to enhance the mechanical and thermal properties of the polymer, where the surface-nucleated crystalline phase has better mechanical and thermal characteristics than the bulk crystal phases. In those cases, using fillers with large surface area maximizes the filler-induced enhancements of the material properties; a dramatic manifestation of such a response is found in nylon-6/montmorillonite nanocomposites.<sup>3–5</sup>

In these nylon-6/inorganic hybrids an addition of a minute amount (2–10 wt %) of montmorillonite (MMT), a nanometer-thin mica-type layered silicate with a surface area of about 750 m<sup>2</sup>/g, was found to cause dramatic enhancements in the materials properties,<sup>5</sup> especially a heat distortion temperature increase of 50–70 K above the bulk nylon-6 value. This increased thermal stability was later attributed to a clay-stabilized  $\gamma$  crystalline phase of nylon-6 formed at the inorganic surface.<sup>3,4</sup> Other examples of property enhancements in polymers that are seen in polymer/layered-silicate hybrids are decreased permeability to gases and liquids, better resistance to solvents, increased thermal stability, improved mechanical properties, and flame retardancy.<sup>6–9</sup> There exist many layered inorganic materials which can have similar effects, when used as fillers in polymer matrices, including synthetic 2:1 aluminosilicates,<sup>10</sup> metal phosphates, transition-metal chalcogenides, layered double hydroxides, and other complex oxides.<sup>11–13</sup>

We have previously shown that PVA/inorganic nanocomposites also possess such filler-induced property enhancements,<sup>9</sup> and those studies suggest the existence of a different crystalline structure, which is created/promoted when sodium montmorillonite (MMT) is added to PVA. At low MMT concentrations, the silicate layers are nearly fully exfoliated, as they become kinetically trapped in the PVA matrix.<sup>9</sup> This allows for the polymer

to be exposed to a large surface area of the inorganic filler, which provides sites on which PVA crystals grow. Inspired by the similarities in property enhancements between nylon-6/mmt hybrids<sup>3–5</sup> and PVA/mmt nanocomposites,<sup>9</sup> we herein study how PVA crystals are affected by the inorganic surfaces.

Namely, we use atomic force microscopy (AFM) techniques to probe the surface crystallization of PVA/mmt nanocomposite films. By complementing the direct imaging obtained from AFM,<sup>14</sup> with X-ray diffraction (XRD) and thermal (DSC) data, we aim to understand the nature of PVA crystals grown next to the inorganic (MMT) surface and how the morphology and/or structure differs from bulk PVA crystals. The present work explores first the different AFM modes that can be used to contrast spatial variations of mechanical properties across a polymer surface. Next, we comparatively apply these modes to study neat PVA film crystal morphology and the effect of the silicate filler surfaces. Finally, on the basis of the AFM results and further data from DSC and XRD, we address the inorganic surface effect on the PVA crystallization. Such an approach shall ultimately provide insights into how materials property changes are connected to the surface-induced changes in the polymer crystal structure/morphology.

**Experimental Section**

**Materials and Sample Preparation.** Sodium montmorillonite (MMT) is a naturally occurring 2:1 phyllosilicate, capable of forming stable suspensions in water. This hydrophilic character of MMT also promotes dispersion of these inorganic crystalline layers in water-soluble polymers such as poly(vinyl alcohol)<sup>9,15</sup> and poly(ethylene oxide).<sup>16–18</sup> Films of neat PVA and PVA/inorganic hybrids were prepared using a film-casting method.<sup>9</sup> Hybrid films were cast from a MMT/water suspension where PVA was dissolved. Room temperature distilled water was used to form a suspension of sodium montmorillonite (Cloisite Na<sup>+</sup>, Southern Clay Products, TX) at a concentration of  $\leq 2.5$  wt %. The suspension was stirred for 1 h and sonicated for 30 min. Low-viscosity (weight-average molecular weight 31 000–50 000 g/mol), commercial grade, fully hydrolyzed (98.0–98.8%), atactic poly(vinyl alcohol) (Airvol 107, Air Products, PA) was added to the stirring suspensions such that the total solids (silicate plus polymer) concentration was  $\leq 5$  wt %. The mixtures were then heated to 90 °C to dissolve the PVA, again sonicated for 30 min, and finally films were cast from solution on top of glass substrates. Drying

\* Corresponding author. E-mail manias@psu.edu.

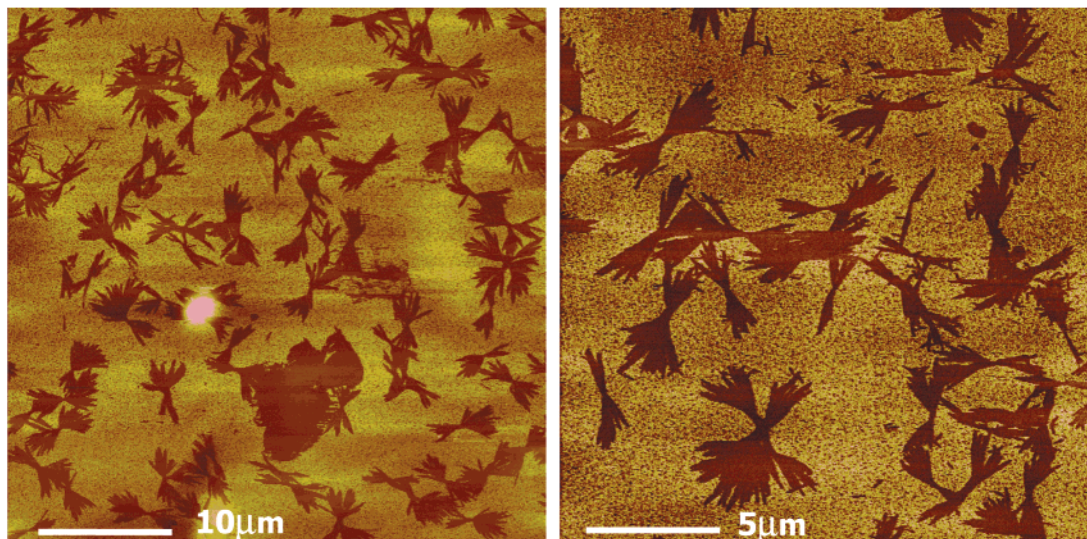


**Figure 1.** AFM images of bulk PVA ( $40 \times 40 \mu\text{m}$  and  $20 \times 20 \mu\text{m}$ ) obtained in contact mode (lateral force images shown). A variety of branched crystal morphologies—nearly impinging—are found throughout the film; however, the same film is nonbirefringent when viewed under a crossed polarized optical microscope.

was done on a hot plate at  $35\text{--}40^\circ\text{C}$ , covered, for 24 h. The nominal film thickness for the AFM samples was  $10 \mu\text{m}$ . Specimens for XRD and DSC studies of neat PVA and PVA/MMT systems were prepared by the same method. The structure and materials properties of these systems are reported elsewhere.<sup>9</sup>

**Characterization.** Atomic force microscopy was performed using a Digital Instruments Multimode AFM, controlled by the Nanoscope IIIa scanning probe microscope controller with a Nanoscope Extender. Three types of tips were used: Nanoprobe Tapping (TESP) and Force Modulation (FESP) SPM tips (both from Digital Instruments, CA) and Ultrasharp Contact (CSC21) tips (from Silicon MDT, Russia). The tapping and force modulation tips are mounted on  $125$  and  $225 \mu\text{m}$  long, single beam cantilevers, with resonant frequencies in the range of  $330\text{--}399$  kHz and  $77\text{--}94$  kHz, respectively, and corresponding spring constants of  $20\text{--}100$  and  $1\text{--}5$  N/m. The contact tip cantilevers are triangular (V-shaped) and have a softer spring constant of typically  $0.12$  N/m.

Differential scanning calorimetry (DSC) was performed in a Perkin-Elmer DSC7 at a heating (or cooling) rate of  $20$  and  $10^\circ\text{C}/\text{min}$  under an argon atmosphere. Wide-angle X-ray diffraction (XRD) data were collected in digital form using a Rigaku Geigerflex powder diffractometer with a Dmax-B controller and a vertical goniometer. Operation was in the  $\theta\text{--}\theta$  geometry. The instrument uses radiation from a copper target tube (Cu  $K\alpha$  radiation,  $\lambda = 1.541871 \text{ \AA}$ , including both the  $K\alpha^1$  and  $K\alpha^2$ , whereas  $K\beta$  was eliminated with a graphite monochromator). We have annealed our samples at  $245^\circ\text{C}$  for 35 min in order to allow for sharper PVA diffracted peaks. Specimens showed some color change; however, the DSC traces of the annealed samples remain the same qualitatively (dual melting peak) and quantitatively (heat of fusion) with those from nonannealed samples.

## Results and Discussion

Our aim in this work is to study the effect of high surface area inorganic fillers on the PVA crystal morphology. For PVA, even when melt crystallized to its fully developed crystal state, cross-polarization optical microscopy cannot be employed, as the crystalline PVA does not have adequate birefringence.<sup>19,20</sup> The same is also the case with our PVA/MMT composites. Moreover, for reasons that will become apparent when discussing our results later, we wanted to focus on the initial stages of PVA crystallization, to identify characteristic differences between the neat and filled systems. In these first

stages of crystallization, we follow submicron size crystals and nuclei developing, a task beyond the resolution of optical microscopy methods.

**PVA Crystallization.** Before we consider the differences between neat and filled PVA systems, we shall briefly discuss how the crystallization of PVA develops in films cast from PVA/water solutions. As cast, these films are mostly amorphous, and crystallites initiate predominately in the final drying stages; crystallization proceeds thereafter slowly, aided by the ambient humidity. If the ambient humidity is too low or absent, the drying polymer becomes glassy, and crystal growth becomes arrested before extended crystallites can develop and impinge. Though PVA has a  $T_g$  above room temperature, water-cast films still form crystals at ambient temperatures due to the slow drying nature of the hydrophilic polymer. Subsequently, plasticization by ambient humidity allows for a slow, cold crystallization of PVA resulting in crystals, which are reminiscent of structures as those from row nucleated crystallization in the earlier stages, dendritic in the mid to latter stages (Figure 1) and spherulitic in final stages after they impinge and fully develop. The final systems include mature crystallites of all these morphologies, and this mixture of morphologies can only be described loosely as PVA dendrites or hedrites<sup>21</sup> due to the branched nature of the crystalline lamellae. These mature crystal structures are still not sufficiently birefringent to be observed with cross-polarization microscopy. Before impinging on each other, the prevailing shape of the PVA crystallites on the surface of the film is a multidirectional “wheat sheaf” structure as shown in Figure 1. These crystallites are not spherulitic, i.e., they do not have a spherulitic symmetry; however, they do conjure up images of young or immature spherulites grown from the melt. The fact that these crystals are grown from water-cast films has no bearing on the fundamental foci of this research; this preparation was only chosen as it allows for crystallization studies at room temperature and over extended time scales.

**Study of Crystals on Polymer Surfaces by AFM.** Since we want to follow the evolution of PVA crystals from the initial stages of crystallization, our approach must provide submicron resolution between crystalline

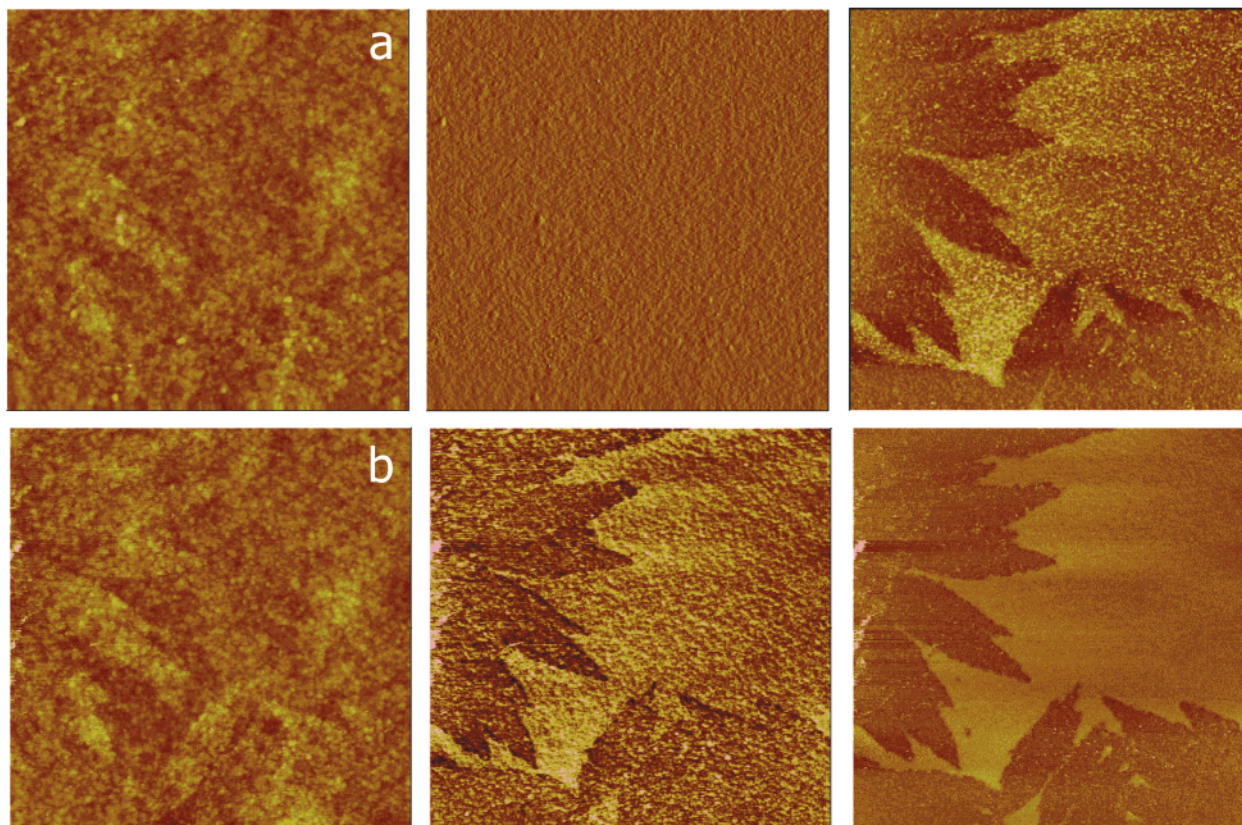


**Figure 2.** AFM imaging of a bulk PVA region ( $5 \times 5 \mu\text{m}$ ) under two intermittent contact modes, obtained with the very same tip. (a) Tapping mode image (left to right: height, amplitude, and phase lag). Small normal forces were used ( $\approx 5 \text{ nN}$ ), and the height image follows closely the topographical features (color scale in height image is  $15 \text{ nm}$ ). The phase lag reflects the difference in stiffness between the crystalline (dark) and amorphous (light) phases. (b) Negative lift force mode image (left to right: height, amplitude, and phase lag) where the height and phase lag are obtained in tapping mode, similar to the images in (a). The amplitude image reflects variations in compressive modulus as the tip indents  $20 \text{ nm}$  below the height profile obtained in the height image; thus, stiffer (crystalline) regions appear darker, whereas the amorphous material appears lighter.

and amorphous regions. Electron microscopy approaches (such as SEM or TEM) cannot provide the needed resolution without catastrophic intervention on the samples (such as etching or chemical staining of the amorphous material). Moreover, optical microscopy methods cannot be used either, due to the PVA nature<sup>19,20</sup> and the need to investigate at the submicron scale. In contrast, AFM can facilitate such studies on polymer surfaces, where mechanical contrast is obtained between hard (crystalline) and softer (amorphous) regions. Apparently, such a contrast necessitates probing the surface in such a way so as to cause a deformation. Crystalline and amorphous regions may be distinguished by probing with a constant force and measuring differences in deformation or alternatively by using a constant deformation and measuring differences in the applied force. Observation of the neat PVA films, as well as films with inorganic fillers, was done using contact mode, tapping mode, and two different force modes. These four AFM modes were chosen in order to elucidate the nature of the growing crystallites as well as to illustrate the fundamental use of the AFM modes.

In contact mode, the normal force applied by the tip on the surface is held constant while the tip is scanned across the sample. This allows the collection of height and lateral force data across the scanned area. In tapping mode, the tip is oscillated in and out of contact with the surface (keeping the maximum force per contact constant and—in our case—small in magnitude) to produce height and phase images; phase lags can

provide a qualitative mapping of mechanical properties. In force modulation modes the tip is again oscillated normal to the sample surface but now probes the sample with higher normal forces, which deform the surface with either constant force or at constant deformation, allowing the collection of height and amplitude data; amplitude now can provide a measure of the modulus or stiffness of the sample. We will discuss in detail how these quantities collected in each mode reflect the topographical and mechanical features of the surfaces. Figures 2 and 3 show a set of images where the same region of a neat PVA film surface was probed in four different modes using the very same tip. These images show the outer growing edges of two young crystallites prior to their full impingement.

The images in Figure 2a were obtained in tapping mode. During tapping mode imaging, the cantilever is excited into oscillation by vibrating the cantilever via a piezoelectric element. Away from the surface the cantilever is driven with a “free oscillation amplitude” (typically  $10\text{--}100 \text{ nm}$ ), subsequently the tip is brought into intermittent contact (tapping) with the surface. The normal force applied to the sample is controlled by setting the oscillation amplitude at contact to be dampened to some fraction of the driving amplitude (“set point amplitude”). Typically, a feedback loop keeps the set point amplitude constant (Figure 2a, middle: amplitude); thus, the tip probes the surface with a constant force. This mode applies almost no lateral forces and allows for imaging with very small normal forces,

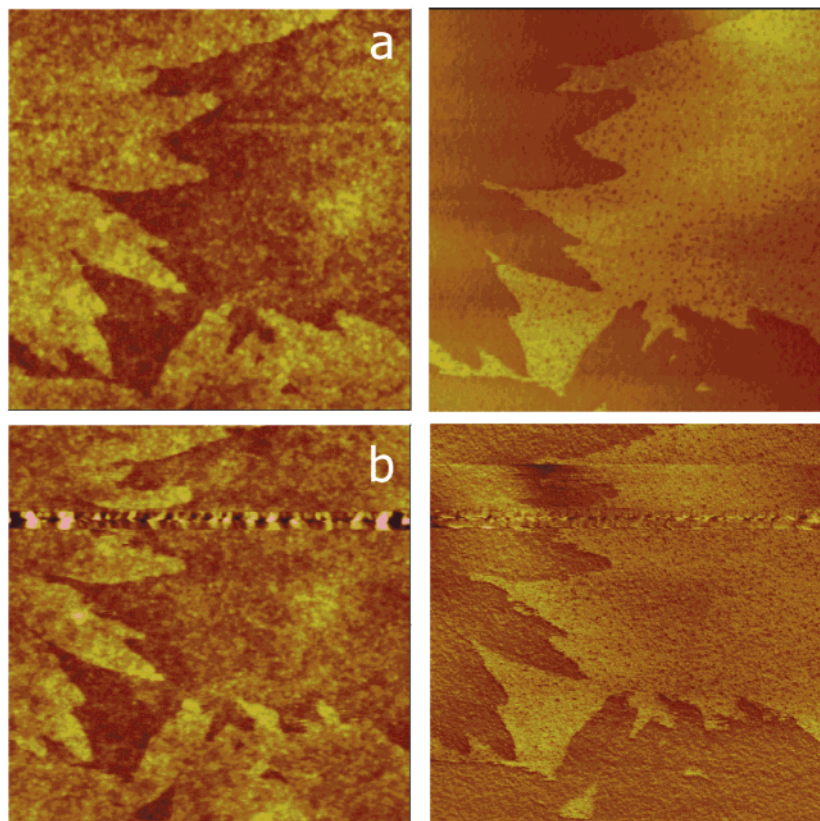


**Figure 3.** The same region as in Figure 1 imaged by the very same tip under larger normal forces. (a) A contact mode image (height left, lateral forces right). The crystalline regions appear in lighter colors in the height and darker in the lateral force scan. (b) A force modulation image (height left, amplitude right). The amplitude, like the amplitude image in Figure 2b, also shows dark contrast for stiffer (crystalline) regions. In both AFM modes, the normal force was constant and larger in magnitude than the forces applied in Figure 2, causing strong deformation of the softer regions, thus appearing “lowered” in the height image. As in the height images of Figure 2, the height color scale is again 15 nm.

thereby creating little or no sample deformation (Figure 2a, left: height). Thus, the tapping mode height (for small applied forces) is a direct measurement of the true surface topography even for soft samples. However, as the tip oscillates in contact with the surface, differences in the mechanical properties across the sample may cause phase lags in the oscillation (much like the viscoelastic mechanical testing of polymers) and thus provide qualitative information about the changes in surface mechanical properties.<sup>22,23</sup> For example, the scan of Figure 2a (right: phase) shows darker contrast (smaller phase shift) for crystalline regions than for amorphous regions. There are many factors affecting the phase shift during tapping mode imaging.<sup>25</sup> In most cases phase inversion can be achieved by varying the amplitude set point, or the driving amplitude, so as to image in the attractive forces regime.<sup>24,25</sup> When tapping in this attractive regime, the phase is sensitive to the tip-sample adhesion, rather than the sample stiffness variation.<sup>25</sup> For PVA investigated at repulsive force set point the crystalline material always appears in dark phase contrast to the amorphous material.

Figures 2b and 3b show two sets of force modulation images. These force modes allow for probing the surface compressive modulus of the sample. During the force mode of Figure 3b, the RMS cantilever deflection is held constant, by adjusting the sample height while the tip indents the sample surface. This slight penetration is done while oscillating the cantilever at 5–10 kHz, a much lower frequency than those in tapping mode (usually >50 kHz). The magnitude of the indentation is dictated by the local compressive modulus. Stiffer

sections of the surface allow less indentation; thus, the cantilever experiences a higher oscillation amplitude than it does on softer sections, which absorb more of the cantilever’s energy resulting in a smaller oscillation amplitude.<sup>26</sup> As can be seen in Figure 3b (right: amplitude), the crystalline regions (stiff) appear in dark contrast to the lighter amorphous regions (more compliant). In this mode, the surface topography effects on the measured amplitude are superimposed on the surface modulus effect (by design of the feedback mechanism used to keep the normal force constant). A quantitative determination of mechanical surface map requires the removal of any topography effects. This is done in Figure 2b under a different force mode (also called “negative lift mode”<sup>26</sup>). The negative lift mode allows for probing with a constant force while maintaining a nearly constant contact area. In other words, the effect of topography is removed from each line scan by scanning each line twice: Namely, the first scan is done with normal tapping mode—such as was used in Figure 2a—thus obtaining the topography of the surface at a high tip-oscillation frequency. During the second scan of the same line the tip indents to a given distance (typically 2–20 nm) below the height profile obtained from the first line scan; in this second pass the tip is also oscillating, but at a low frequency (5–10 kHz). The result is that, by eliminating the topography from each scan, the force set point remains constant, and the tip probes nearly the same distance into the sample at each pass, allowing the contact area between the tip and sample to remain constant. This provides a more pure representation of the relative compressive moduli across

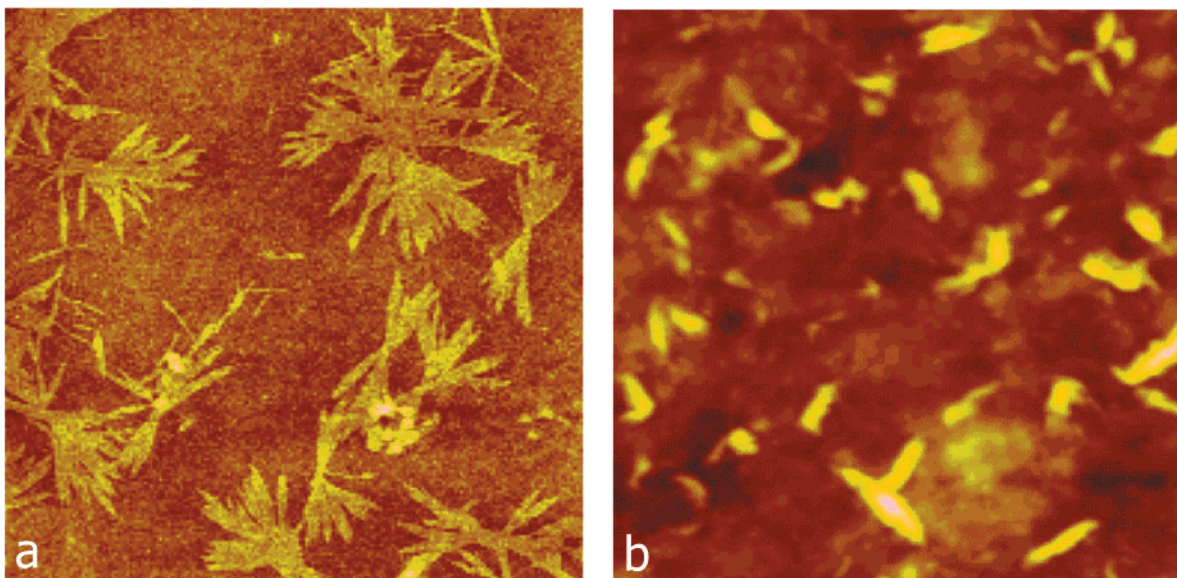


**Figure 4.** Comparison between bulk PVA (a) and PVA/4 wt % MMT (b), both  $15 \times 15 \mu\text{m}$ . Contact mode (height) images are shown under the high normal forces, for which crystalline material appears in lighter colors, since it undergoes smaller deformations. The modulus of the amorphous polymer in the PVA/MMT system (b) is much higher (almost a 3-fold<sup>9</sup>) than the amorphous bulk (a), resulting in much smaller deformation under the same normal force and thus in less contrast of the “apparent topography”. There is a marked decrease in crystallite size and a change in shape when submicron inorganic particles are introduced in the PVA.

the scanned area.<sup>27</sup> As can be seen in Figure 2b, the crystalline regions appear in dark contrast to the amorphous regions. Phase data are collected during the first—tapping mode—line scan.

The variation in surface elasticity across the scanned area also causes apparent differences to the height image.<sup>28,29</sup> As the sample is probed by the tip at a constant force, soft regions will deform more than stiff regions. Thus, soft regions will appear to be lower in height. For a given sample, this apparent height difference—which is added to the topography features in the height images—depends on the magnitude of the applied normal force. This is evident in the height images of Figures 2 and 3: The topography is relatively featureless (as seen in Figure 2a/height), but as the normal force increases, the sample deforms more, and this deformation appears as an increasing height difference between the softer and stiffer regions in the height images. In Figures 2 and 3 the normal force increases in the following order: 2a, 2b, 3b, 3a, and it is easily observed that the “height contrast” between softer and harder regions also increases in the same way (the scale is 15 nm for all the height images of Figures 2 and 3). Exactly the same effect can be seen in the tapping mode height images by decreasing the set point (i.e., increasing the applied normal force), and the height image changes from an almost pure “topography” mapping to an image where stiffer regions appear higher.

Finally, tapping and force mode imaging may be complemented by “contact mode” scans as shown in Figure 3a. In the contact mode, the tip is not oscillated but rather is scanned across the sample in constant contact with it. The applied normal force can be held constant and is much larger than the tapping mode normal force. As discussed above, the height image obtained contains both topographical and “mechanical” features. Because the tip is dragged along the surface, lateral forces can also be measured while scanning. It has been shown that the crystalline regions of typical semicrystalline polymers have a lower coefficient of

friction, compared to the amorphous regions.<sup>24</sup> In Figure 3a the same region as that of Figures 2 and 3b is imaged in contact mode, and the crystalline material has a lower lateral force than the surrounding amorphous material. In summary, from the discussion of Figures 2 and 3 it becomes obvious that the sample topography can be obtained from tapping mode when high set points (i.e., low forces) are used, whereas mechanical property mappings can be obtained through the amplitude of force modulation mode, phase differences of tapping mode, and lateral forces of contact mode. In most of these AFM images several surface features are superimposed (including topography features and gradients as well as changes in the surface modulus), and only through comparative AFM scans with multiple modes can each of these components be resolved.

**Crystal Morphology.** AFM was performed in all the above modes on bulk PVA films and on PVA filled with inorganic layers (4, 10, and 20 wt % MMT) in order to measure differences in crystal morphology, with the emphasis on the initial stages of crystallization. As can be seen in Figure 4a, the bulk PVA has crystals which grow to sizes of about  $5 \mu\text{m}$  and larger, before impinging upon neighboring crystallites and arresting further growth. In contrast, when inorganic filler layers are present (Figure 4b), the crystallites are smaller and more linear in shape than the bulk crystallites. Crystallite sizes in the MMT-filled system are about  $1\text{--}2 \mu\text{m}$ , when grown in the vicinity of the inorganic particles. The color scales used in both images show the crystalline regions in lighter color, corresponding to higher apparent topography (i.e., smaller deformation under the constant applied force in addition to any true topography features). The behavior of PVA systems loaded with 10 and 20% MMT is similar to that of Figure 4b; i.e., crystals grow in a linear fashion, albeit in much higher density on the surface. Because of the higher crystallite densities, the crystalline regions overlap, making it impossible to assign a diameter or length to these structures.

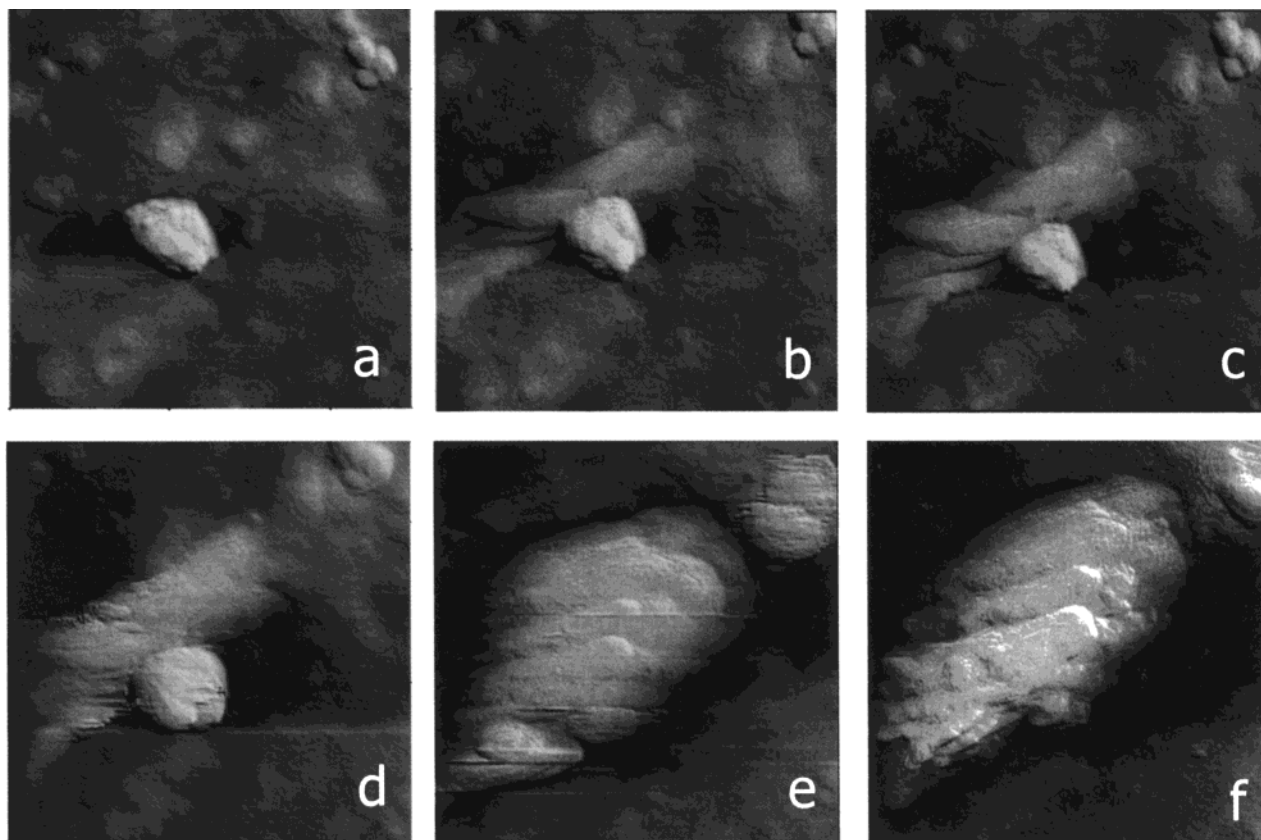


**Figure 5.** A time series of height images ( $2.5 \times 2.5 \mu\text{m}$ ), obtained by tapping mode AFM in the vicinity of a protuberant inorganic filler tactoid. Time after casting is as follows: (a) 36 h, (b) 3 days, (c) 4 days, (d) 6 days, (e) 20 days, and (f) 21 days. The height scale (light to dark) is 400 nm (a–d) and 500 nm (e, f). The PVA crystal initiates next to the inorganic surface (a), grows in size (b–d), and eventually covers completely the surface of the silicate (e). The same crystallization behavior observed near the central protuberant tactoid can also be seen for a smaller inorganic particle in the top right corner.

To elucidate the crystallization mechanisms responsible for this difference in morphology, we followed the evolution of the PVA crystals growing next to silicate layers or tactoids. (The silicate particles imaged can be easily designated as layers or tactoids through their size: single layers are 1 nm thin, whereas tactoids—stacks of parallel packed single layers—are much larger, on the order of 100 nm.) In Figure 5, we follow the time evolution of PVA crystals in a  $2.5 \times 2.5 \mu\text{m}$  region of a PVA/4 wt % MMT sample, at room temperature<sup>30</sup> and 50% relative humidity. This image depicts well the general behavior found in the silicate filled system; i.e., the crystalline material found in Figure 5 is indicative of the crystallites found in most images of the PVA/silicate systems studied here, as is evident in Figure 4. Figure 5 shows a time series of height images, obtained by tapping AFM in the vicinity of a protuberant inorganic filler particle (a tactoid in this case). The crystalline PVA regions correspond to the apparent “higher” features in Figure 5; concurrent phase and force imaging show that these “higher” features are much more stiff than the surrounding material, which is also confirmed by subsequent lateral force contact imaging. Thus, we may safely conclude that the light-colored material is crystalline, and the darker-colored regions are amorphous. The PVA crystal initiates next to the inorganic surface (a), grows in size (b–d), and eventually covers completely the surface of the silicate (e). Furthermore, once the silicate becomes covered with PVA, it appears to continue to recruit amorphous polymer for crystallization in the same region (f), albeit slower than before. The tendency of the PVA to com-

pletely cover the tactoid in Figure 5, which is typical also in all other regions of this sample, is driven by the strong specific interactions between the PVA and the silicate,<sup>9</sup> which cause a strong wetting of the polymer on the inorganic surface. The fact that these crystals grow in a linear fashion suggests that nucleation prefers to begin near the inorganic surface and that, once nucleated, the crystals tend to grow upon one another.

The PVA vinyl alcohol group forms hydrogen bonds with the silicate oxygens, which dominate the cleavage plane of MMT. Moreover, due to the atomically smooth MMT surface, these specific interactions are expected to force chains to create long adsorbed trains,<sup>31</sup> which in turn will promote a strongly interacting second layer of PVA to crystallize on top of them. Thus, this MMT surface epitaxial/nucleating effect can be “felt” through many layers of polymer, causing a long-range collection and crystallization of PVA from the surface of the silicate (Figure 5). Therefore, these sites tend to act as nucleating sites for the PVA crystallites. Accordingly, scans of the PVA/4 wt % MMT show many more crystallites per area compared to the neat PVA, as all the inorganic silicate fillers nucleate polymer crystallites. The PVA/MMT specific interactions decrease the surface energy necessary to create/nucleate a polymer crystal, and thus, the crystalline regions tend to nucleate around the silicate surfaces. Furthermore, since the silicate surface can be felt through only a small distance, the new crystallites formed only grow to a limited size of about  $2 \mu\text{m}$ . Hence, it is not unexpected that the size falls from  $5 \mu\text{m}$ , in the neat PVA, to  $1\text{--}2 \mu\text{m}$  in the MMT filled PVA (Figure 4).

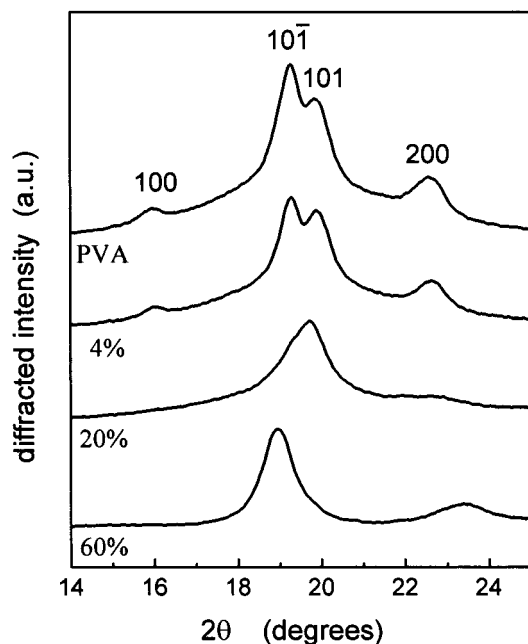


**Figure 6.** XRD curves of bulk PVA and silicate filled composites of various inorganic compositions. The bulk PVA reflections (100, 101, 101, and 200) are at  $2\theta = 16.0^\circ$ ,  $19.4^\circ$ ,  $20.1^\circ$ , and  $22.7^\circ$ , respectively. With increasing inorganic content, there appears a concerted decrease in intensity of the 101 and 101 peaks, accompanied by the appearance of a new peak centered at  $2\theta = 19.5^\circ$ , suggesting a new crystalline form for the clay-induced PVA crystals.

**Crystal Nature.** Wide-angle XRD provides evidence that not only the crystal morphology but also the crystalline structure changes when the inorganic filler is added to PVA. Namely, in the  $2\theta$  region between  $14.0^\circ$  and  $25.5^\circ$  (Figure 6) PVA has its 100, 101, 101, and 200 crystalline reflections (corresponding to  $2\theta = 16.0^\circ$ ,  $19.4^\circ$ ,  $20.1^\circ$ , and  $22.7^\circ$ , respectively). The XRD scans in Figure 6 (neat PVA and 4, 20, and 60 wt % MMT) suggest that as silicate content increases from  $\phi_{\text{MMT}} = 0$  to 20 wt %, the 101 and 101 peaks show a concerted decrease in intensity. This depression of the 101 and 101 peaks is accompanied by the appearance of a single peak centered at  $2\theta \approx 19.5^\circ$ . This development of the diffraction peaks indicates that a new crystal structure forms with the addition of the silicate, at the expense of the bulklike crystal structure.<sup>32</sup> Given the multiple overlapping peaks in the diffraction pattern, it is difficult to quantify with any accuracy neither the difference of the crystallite sizes,<sup>33</sup> nor the simultaneous change in crystalline structure. However, the bulklike and filler-induced crystals also have different melting temperatures ( $T_m$ ), and DSC can be employed to quantify the change in crystalline structure with  $\phi_{\text{MMT}}$ .

In Figure 7b, DSC traces are shown for the melting transitions of neat PVA films as well as PVA films filled with MMT. Bulk PVA has a melting transition at  $T_m \approx 225^\circ\text{C}$ . As inorganic layers are added to PVA the polymer crystallinity does not change markedly; however, a new, higher  $T_m$  crystalline form appears (Figure 7b). Figure 7a shows the inorganic content dependence of the fractions of the two melting transitions; these fractions are defined via the ratios of the corresponding enthalpies of melting over the total enthalpy of the sample, both for the bulklike  $T_m$  and for the new—higher  $T_m$ —melting transition observed in the presence of the inorganic fillers. Figure 7a clearly indicates that the presence of the inorganic surface induces a new higher

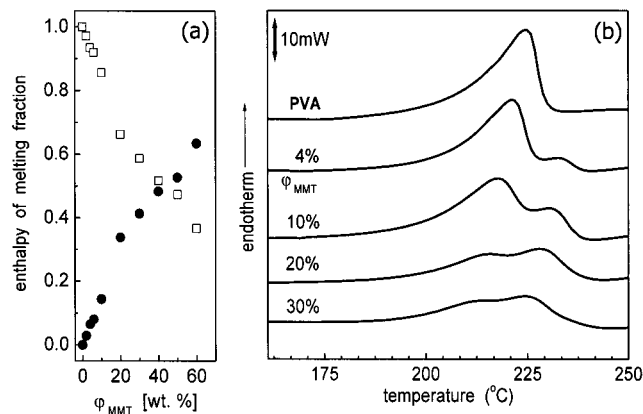


**Figure 7.** DSC traces showing the melting region of PVA/silicate composites of various chosen compositions. On the left, the fractions of the two melting enthalpies for the two crystalline forms for all the MMT concentrations studied [squares, bulklike crystal ( $T_m \approx 225^\circ\text{C}$ ); circles, higher  $T_m$  crystal]. The dependence of the enthalpy fractions on the  $\phi_{\text{MMT}}$  suggests that the inorganic surface promotes a new, higher  $T_m$  crystal form, at the expense of the bulk crystalline material.

$T_m$  crystal at the expense of the bulklike crystals. This behavior is consistent with the XRD observation (Figure 6) of a new crystal phase that gradually appears with the addition of the fillers, with a parallel depression of the bulklike crystal peaks. Our AFM scans (Figure 5) show that the inorganic-induced crystals grow around the inorganic fillers, and this suggests that the higher  $T_m$  may originate from the specific interactions near the PVA/silicate interface, which result in a strong polymer/inorganic adhesion.

## Conclusions

Using AFM, we have investigated the differences in neat PVA films and PVA films filled by MMT inorganic layers. Mechanical variations across polymer surfaces—as those between amorphous and crystalline regions—are manifested in various AFM imaging modes, including contact, intermittent contact, and two force modes. Since in most cases the mechanical variations are superimposed on surface topographical features, oftentimes comparative imaging with various modes is needed to unambiguously resolve polymer crystal, amorphous polymer, and filler particles.

When inorganic layers (MMT) are added to the PVA polymer, crystallites are initiated and grown in the immediate vicinity of the inorganic surface. We believe that this is due to the strong specific interactions between the inorganic surfaces and the polymer. The crystallites found near the inorganic fillers are about  $2\ \mu\text{m}$  in size, smaller than the crystallites found in the neat PVA film, which are  $5\ \mu\text{m}$  or larger. Moreover, the melting temperature of these crystals was found to be higher than the bulk  $T_m$ . At the same time, XRD also shows differences in the PVA crystalline structure when crystallized in the presence of MMT, suggesting that the inorganic fillers change also the crystal structure. This new, silicate-induced PVA crystal phase is promoted by the existence of the montmorillonite layers and forms at the expense of the bulk PVA crystalline phase.

**Acknowledgment.** This work is supported by ACS/PRF (Grant 37274-G5) and the AFM instrumentation by NSF (Contract DMR-9975624). We thankfully ac-

knowledge J. Runt and V. Koutsos for helpful discussions and the anonymous reviewers for the critical reading of the manuscript.

## References and Notes

- Bassett, D. C. *Principles of Polymer Morphology*; Cambridge University Press: Cambridge, 1981. Lee, J.-C.; Nakajima, K.; Ikehara, T.; Nishi, T. *J. Appl. Polym. Sci.* **1997**, *64*, 797. Mi, Y.; Chen, X.; Guo, Q. *J. Appl. Polym. Sci.* **1997**, *64*, 1267. Wang, C.; Chen, C.-C. *Polym. Bull.* **1999**, *43*, 433. Mucha, M.; Marszalek, J.; Fidrych, A. *Polymer* **2000**, *41*, 4137. Stocker, W.; Schumacher, M.; Graff, S.; Thierry, A.; Wittmann, J.-C.; Lotz, B. *Macromolecules* **1998**, *31*, 807. Doye, J. P. K.; Frenkel, D. *J. Chem. Phys.* **1998**, *109*, 10033.
- Janigova, I.; Chodak, I. *Eur. Polym. J.* **1995**, *31*, 271. Liang, J. Z.; Li, R. K. Y.; Tjong, S. C. *J. Appl. Polym. Sci.* **1999**, *71*, 687. Tjong, S. C.; Xu, S. A. *Polym. Int.* **1997**, *44*, 95. Alonso, M.; Velasco, J. I.; de Saja, J. A. *Eur. Polym. J.* **1997**, *33*, 255. Radhakrishnan, S.; Saujanya, C. *J. Mater. Sci.* **1997**, *64*, 1267. Stricker, F.; Bruch, M.; Mulhaupt, R. *Polymer* **1997**, *38*, 5347. Trifonova, D.; Varga, J.; Vancso, G. J. *Polym. Mater. Sci. Eng.* **1998**, *41*, 341.
- Liu, L.; Qi, Z.; Zhu, X. *J. Appl. Polym. Sci.* **1999**, *71*, 1133.
- Davis, R. D.; Jarrett, W. L.; Mathias, L. J. *Polym. Mater. Sci. Eng.* **2000**, *82*, 272.
- Kojima, Y.; Usuki, A.; Kawasumi, M.; Okada, A.; Kurauchi, T. T.; Kamigaito, O. *J. Polym. Sci., Part A: Polym. Chem.* **1993**, *31*, 983. Kojima, Y.; et al. *J. Polym. Sci., Part B: Polym. Phys.* **1995**, *33*, 1039.
- Krishnamoorti, R. K.; Vaia, R. A.; Giannelis, E. P. *Chem. Mater.* **1996**, *8*, 1728. Giannelis, E. P. *Adv. Mater.* **1996**, *8*, 29.
- Alexandre, M.; Dubois, P. *Mater. Sci. Eng., R* **2000**, *28*, 1.
- Gilman, J. W.; Jackson, C. L.; Morgan, A. B.; Harris, R.; Manias, E.; Giannelis, E. P.; Wuthenow, M.; Hilton, D.; Philips, S. H. *Chem. Mater.* **2000**, *12*, 1866.
- Strawhecker, K.; Manias, E. *Chem. Mater.* **2000**, *12*, 2943.
- Giannelis, E. P.; Krishnamoorti, R. K.; Manias, E. *Adv. Polym. Sci.* **1998**, *138*, 107.
- Lan, T.; Kaviratna, P. D.; Pinnavaia, T. J. *Chem. Mater.* **1995**, *7*, 2144. Wang, M. S.; Pinnavaia, T. J. *Chem. Mater.* **1994**, *6*, 2216. Pinnavaia, T. J. *Science* **1983**, *220*, 365.
- Kanatzidis, M. G.; Wu, C.-G.; Marcy, H. O.; DeGroot, D. C.; Kannewurf, C. R. *Chem. Mater.* **1990**, *2*, 222; **1991**, *3*, 992; **1996**, *8*, 525.
- Vaia, R. A.; Ishii, H.; Giannelis, E. P. *Chem. Mater.* **1993**, *5*, 1694. Vaia, R. A.; Jandt, K. D.; Kramer, E. J.; Giannelis, E. P. *Macromolecules* **1995**, *28*, 8080. Vaia, R. A.; Price, G.; Ruth, P.; Nguyen, H. T.; Lichtenhan, J. *Appl. Clay Sci.* **1999**, *15*, 67.
- Limary, R.; Swinnea, S.; Green, P. F. *Macromolecules* **2000**, *33*, 5227.
- Carrado, K. A.; Thiyagarajan, P.; Elder, D. L. *Clays Clay Mineral.* **1996**, *44*, 506.
- Vaia, R. A.; Vasudevan, S.; Krawiec, W.; Scanlon, L. G.; Giannelis, E. P. *Adv. Mater.* **1995**, *7*, 154; *J. Polym. Sci., Part B: Polym. Phys.* **1997**, *35*, 59.
- Wong, S.; Vasudevan, S.; Vaia, R. A.; Giannelis, E. P.; Zax, D. B. *Solid State Ionics* **1996**, *86*, 547.
- Hackett, E.; Manias, E.; Giannelis, E. P. *Chem. Mater.* **2000**, *12*, 2161.
- Finch, C. A. *Polyvinyl alcohol*; John Wiley & Sons: New York, 1992.
- Fukae, R.; Yamamoto, T.; Fujita, Y.; Kawatsuki, N.; Sangen, O.; Kamachi, M. *Polym. J.* **1997**, *29*, 293. Assender, H. E.; Windle, A. H. *Polymer* **1998**, *39*, 4295. Cho, J. D.; Lyoo, W. S.; Chvalun, S. N.; Blackwell, J. *Macromolecules* **1999**, *32*, 6236.
- Woodward, A. E. *Principles of Polymer Morphology*; Cambridge University Press: Cambridge, 1981.
- Quantitative mechanical information can also be obtained; however, one has to go beyond the instrument's commercial imaging/operation software capabilities.<sup>23</sup>
- Fretigny, C.; Basire, C.; Granier, V. *J. Appl. Phys.* **1997**, *82*, 43.
- Ratner, B.; Tsukruk, V. V. *Scanning Probe Microscopy of Polymers*; ACS Symposium Series 694; American Chemical Society: Washington, DC, 1998.
- Magonov, S. N.; Elings, V.; Whangbo, M.-H. *Surf. Sci.* **1997**, *375*, L385. Bar, G.; Thomann, Y.; Brandsch, R.; Cantow, H.-J. *Langmuir* **1997**, *13*, 3807. Schmitz, I.; Schreiner, M.; Friedbacher, G.; Grasserbauer, M. *Appl. Surf. Sci.* **1997**, *115*, 190. Pickering, J. P.; Vancso, G. J. *Polym. Bull.* **1998**, *40*, 549.
- Force modulation application note*; Digital Instruments: Santa Barbara, 1998.
- The relative compression modulus between different regions in the scanned area can be quantified by this mode. Absolute moduli can be also obtained, where regions/components of the sample are of a known surface modulus or, alternatively, by scanning with the same tip and with the same scanning parameters a different surface of known surface modulus.
- Chizhik, S. A.; Huang, Z.; Gorbunov, V. V.; Myshkin, N. K.; Tsukruk, V. V. *Langmuir* **1998**, *14*, 2606.
- Gracias, D. H.; Somorjai, G. A. *Macromolecules* **1998**, *31*, 1269.
- PVA crystallization does take place at room temperature (although  $T_c^{PVA} = 193$  °C) because of the strong PVA hydrophilicity: At room temperature PVA tends to absorb water from the ambient humidity—especially at the free surface—which leads to a dilution/plasticization effect, which promotes crystallization far below  $T_c^{PVA}$ .
- Israelachvili, J. *Intermolecular and Surface Forces*; Academic Press: London, 1991.
- The XRD of the neat MMT is not given in Figure 6 for clarity. The appearance of the new peak, observed in the higher loading PVA/MMT systems, is not connected in any way with the crystalline reflections from the MMT structure.
- Guinier, A. *X-ray Diffraction in Crystals, Imperfect Crystals, and Amorphous Bodies*; W. H. Freeman: San Francisco, 1963.

MA0101862